

High cloud properties from three years of MODIS Terra and Aqua Collection 4
Data over the Tropics

Gang Hong and Ping Yang

Department of Atmospheric Sciences, Texas A&M University, College Station, TX
77843, USA

Bo-Cai Gao

Remote Sensing Division, Naval Research Laboratory, Washington, DC 20375, USA

Bryan A. Baum

Space Science and Engineering Center, University of Wisconsin-Madison, Madison, WI
53706, USA

Yong X. Hu

NASA Langley Research Center, Hampton, VA 23681, USA

Michael D. King and Steven Platnick

NASA Goddard Space Flight Center, Greenbelt, MD 20711, USA

Corresponding author address: Dr. Ping Yang, Department of Atmospheric Sciences,
Texas A&M University, College Station, TX 77843; Tel: 979-845-4923.
Email: pyang@ariel.met.tamu.edu

Abstract

This study surveys the optical and microphysical properties of high (ice) clouds over the tropics (30°S – 30°N) over a 3-year period from September 2002 through August 2005. The analyses are based on the gridded Level-3 cloud products derived from the measurements acquired by the Moderate Resolution Imaging Spectroradiometer (MODIS) instruments aboard both the NASA Earth Observing System Terra and Aqua platforms. The present analysis is based on the MODIS Collection 4 data products. The cloud products provide daily, weekly, and monthly mean cloud fraction, cloud optical thickness, cloud effective radius, cloud-top temperature, cloud-top pressure, and cloud effective emissivity that is defined as the product of cloud emittance and cloud fraction. This study is focused on high-level ice clouds. The MODIS-derived high clouds are classified as cirriform and deep convective clouds using the International Satellite Cloud Climatology Project (ISCCP) classification scheme. Cirriform clouds comprise more than 80% of the total high clouds, whereas deep convective clouds account for less than 20% of the total high clouds. High clouds are prevalent over the Intertropical Convergence Zone (ITCZ), the South Pacific Convergence Zone (SPCZ), tropical Africa, Indian Ocean, tropical America, and South America. Moreover, land-ocean, morning-afternoon, and summer-winter variations of high cloud properties are also observed.

1. Introduction

High clouds occur frequently over the tropics (e.g., Liou 1986; Rossow and Schiffer 1999; Wylie et al. 1994; Liu et al. 1995; Wang et al. 1996, 1998; Wylie and Menzel 1999; Dessler and Yang 2003; Luo and Rossow 2004; Wylie et al., 2005; Stubenrauch et al., 2006). The effect of high clouds on the climate system is highly sensitive to their optical and microphysical properties (e.g., Stephens et al. 1990; Liu and Curry 1999; McFarquhar et al. 2002). Cloud parameterizations in climate models need to account properly for the temporal and spatial distributions of high cloud properties (Tselioudis and Jakob 2002; Ringer and Allan 2004; Lin and Zhang 2004; Li et al. 2005). The representation of tropical high clouds in General Circulation Models (GCMs) has been evaluated (Lin and Zhang 2004; Zhang et al. 2005; Li et al. 2005). Zhang et al. (2005) compared basic cloud climatologies from ten GCMs with satellite measurements from the International Satellite Cloud Climatology Project (ISCCP, Schiffer and Rossow 1983; Rossow and Schiffer 1991, 1999) and the Clouds and Earth's Radiant Energy System (CERES, Wielicki et al. 1996) missions. Significant differences between the model simulations and measurements were found.

This study is intended to investigate the characteristics of high clouds based on cloud products derived from the measurements acquired by the Moderate Resolution Imaging Spectroradiometer (MODIS) sensors (Salomonson et al. 1989; Barnes et al. 1998) on NASA's Earth Observing System (EOS) Terra and Aqua platforms over a three-year period. The MODIS sensors provide unique capabilities to investigate cloud properties from space observations. In addition to cloud fraction, cloud-top temperature, cloud-top pressure, and effective cloud amount, MODIS also provides information about

thermodynamic cloud phase, optical thickness, and effective radius. The optical thickness and effective radius are used to estimate ice water path, a parameter of interest to weather forecasters and climate modelers.

Stephens et al. (1990) investigated the relevance of the microphysical and radiative properties of cirrus clouds to climate and climatic feedback. It was found that the influence of cirrus clouds on climate was affected strongly by the values of effective radius and asymmetry parameter. Effective radius has been suggested to be a function of ice water content and/or cloud temperature (McFarlane et al. 1992; Ou and Liou 1995; Wyser 1998). The effect of ice cloud feedback on GCM simulations can be either positive or negative, depending on the value of effective radius assumed (Jensen et al. 1994; Lubin et al. 1998). Other studies have suggested that ice cloud forcing is sensitive to both ice effective radius and optical thickness (Pilewskie and Valero, 1996; Chung et al., 2000; and Wendisch et al., 2005).

Most, but not all, of the MODIS cloud properties are provided in other satellite-based cloud climatologies. For example, Wylie et al. (2005) investigate the frequency, geographical distribution, and temporal variations of upper tropospheric clouds using 22 years (from 1979 to 2001) of NOAA polar-orbiting High-Resolution Infrared Radiometer Sounder (HIRS/2) multispectral data. The HIRS/2 has a nominal field of view (FOV) of approximately 17 km at nadir. The HIRS/2 cirrus climatology reports on the geographical and seasonal distributions of cloud fraction, cloud-top pressure, and effective cloud amount (cloud fraction N multiplied by cloud emittance ϵ). While clouds were found globally in 75% of the HIRS data, high clouds (cloud-top pressure $P_c < 440$ hPa) were found in 33% of the cloudy FOVs. Furthermore, 15%, 15%, and 3% of these high clouds

were transmissive ($N\epsilon < 0.5$), thick ($0.5 < N\epsilon < 0.95$), and opaque ($N\epsilon > 0.95$), respectively.

The ISCCP has produced over twenty years of cloud products with a spatial resolution of 20 km and a temporal resolution of 3 hours (Schiffer and Rossow 1983; Rossow and Schiffer 1991, 1999). The ISCCP products contain various cloud optical and microphysical parameters, including cloud fraction, cloud-top temperature, cloud-top pressure, optical thickness, and water path, available from the ISCCP C-series and D-series (Rossow and Schiffer 1999). However, the information about cloud effective radius is quite limited because only one particle size is assumed for water clouds and another for ice clouds. Specifically, water clouds are assumed to be composed of liquid water droplets (spheres) with an effective radius of 10 μm , while ice clouds are composed solely of fractal polycrystals (Macke et al., 1996) with an effective radius of 30 μm (Rossow and Schiffer 1999). A cloud is assumed to be composed solely of ice particles when the cloud-top temperature is less than 260 K. According to the ISCCP cloud products, high clouds cover approximately 22% of the globe and 24% of the tropics.

Stubenrauch et al. (2006) analyzed eight years (1987–1995) of TIROS-N Observational Vertical Sounder (TOVS) Pathfinder B (hereafter, referred as TOVS Path-B) data from the NOAA polar orbiting satellites. The TOVS Path-B analyses indicate that cirrus clouds cover approximately 27% of the globe and 45% of the tropics. These results are similar to those of Wylie et al. (2005). The frequency of high clouds derived by Stubenrauch et al. (2006) and Wylie et al. (2005) is larger than that from ISCCP.

There are currently two MODIS imagers in operation, one each on the Terra and Aqua platforms. The EOS Terra platform was launched in December 1999, while the

Aqua platform was launched in May 2002. MODIS measures radiances in 36 spectral bands at wavelengths from 0.4 to 14.2 μm and has a swath width of 2330 km. The spatial resolution at nadir ranges from 250 m to 1 km depending on the wavelength. MODIS has a repeat cycle of 16 days, and global coverage can be obtained in approximately 2 days. The coverage of key atmospheric bands by the MODIS instruments largely enhances the capability of remote sensing of high clouds from space-borne observations (King et al. 2003; Platnick et al. 2003). In terms of the retrieval of the ice cloud optical thickness and effective radius retrievals, the Collection 4 MODIS cloud products are based on the ice cloud optical models (Baum et al. 2000; King et al. 2004) that account for a mixture of various ice habits whose single-scattering properties are computed from the methods reported by Yang and Liou (1996a, b). Recently new ice cloud bulk scattering models (Baum et al. 2005a, b) have been developed and are being used operationally for the Collection 5 MODIS cloud products. However, as only Collection 4 was available when this study was carried out, the present analyses are based on Collection 4 products.

Based on the three years of the MODIS cloud products, we investigate high cloud properties over the tropics (30°S–30°N). Section 2 briefly describes the MODIS high cloud products and the classification of cirriform and deep convective clouds. Three-year mean properties and monthly variations of high clouds are analyzed in Section 3.1. Geographical distributions and seasonal variation of high clouds are analyzed in Sections 3.2 and 3.3, respectively. In Section 3.4, we investigate the zonal means of high cloud properties with latitudes. Section 4 summarizes this study.

2. Data and methodology

The present analyses are based on the MODIS Collection 4 data sets. The MODIS operational cloud retrieval algorithm was recently improved and new data sets (Collection 5) have been released (King et al. 2006). In addition to several other significant improvements on the MODIS ice cloud retrievals, the look-up tables of the bidirectional reflectances, transmittances, and spherical albedos of ice clouds (the so-called ice libraries) have been improved for the MODIS Collection 5 cloud property retrievals. Specifically, new ice crystal size and habit distribution models have been used in the development of the new ice libraries (Baum et al. 2005). Additionally, improved treatments for small ice crystals have also been incorporated in the MODIS Collection 5 ice libraries. King et al. (2006) reported that the effective radii from Collection 5 may be a few micrometers smaller than those in Collection 4. Furthermore, the ice cloud optical thicknesses in the Collection 5 may be slightly larger than those in the Collection 4. Those changes would not substantially impact the analyses of the geographical distributions and seasonal variations of ice cloud properties, which, however, could have a potential impact on the land-ocean and morning-afternoon contrast of high cloud properties and also on the assessment of the radiative forcing of these clouds.

The daily MODIS Level-3 atmosphere products (MOD08_D3 and MYD08_D3) from the Terra and Aqua measurements contain roughly 600 statistical datasets (King et al. 2003). The Level-3 products are derived from four Level-2 atmosphere products including aerosol properties (MOD04), precipitable water (MOD05), cloud properties (MOD06), and atmospheric profiles (MOD07). The MOD06 combines infrared and visible techniques to determine both physical and radiative cloud properties (Platnick et al. 2003). The CO₂ slicing technique (Menzel et al. 1983; Wylie and Menzel 1999) has

been used to infer cloud-top pressure, temperature, and effective emissivity with a $5 \text{ km} \times 5 \text{ km}$ spatial resolution at nadir using MODIS bands 31 and 33-36. The optical thickness and effective radius are derived from the MODIS water-absorbing bands (1.6, 2.1, and $3.7 \text{ }\mu\text{m}$) in conjunction with the nonabsorbing bands (0.65 , 0.86 , and $1.2 \text{ }\mu\text{m}$). The MOD08_D3 (MYD08_D3) products are aggregated with a $1^\circ \times 1^\circ$ (longitude and latitude) spatial resolution over the globe. Three years of the daily MOD08_D3 and MYD08_D3 data from September 2002 to August 2005 over the tropics (between 30°S and 30°N) are used in the present analysis.

The simple statistics of the mean or QA-weighted mean of high cloud properties within each grid cell is available from the MOD08_D3 (MYD08_D3) products. For the QA-weighted mean, each retrieval is weighted by a QA integer (0 to 3) (Platnick et al, 2003). The high cloud optical thickness and effective radius derived from the MODIS visible and near-infrared channel radiances are taken directly from the QA-weighted means in the MOD08_D3 (MYD08_D3) products. Cloud-top pressure, cloud-top temperature, and effective emissivity are also provided in the MOD08_D3 (MYD08_D3) products. The mean cloud fraction can be derived from the ratio of the counts flagged as cloudy to the total observations within each grid cell in the studied time period. The cloud optical thickness is the visible extinction optical thickness. The effective particle radius for the MODIS operational cloud retrievals is defined as follows (King et al. 2003):

$$r_e = \frac{3 \int V(D)n(D)dD}{4 \int A(D)n(D)dD}, \quad (1)$$

where D , V , and A denote the maximum dimension, volume, and projected area of an ice particle, respectively. In Eq. (1), the quantity $n(D)$ indicates the size distribution of ice

particles. Note that the definition of the effective particle radius, in terms of the ratio of the total volume to the total projected area, can be traced back to the study by Foot (1998).

We also study the properties of cirriform and deep convective clouds. The ISCCP scheme (Rossow and Schiffer 1999) classifies a pixel as being high cloud (presumably ice) if the cloud-top pressure is less than 440 hPa, and further categorizes the cloud as being cirrus, cirrostratus, or deep convective cloud. A cirrus cloud is defined as a high cloud with an optical thickness (τ) less than 3.6. A cirrostratus cloud is defined as a high cloud with $3.6 < \tau < 23.0$. A deep convective cloud is defined as a high cloud with $\tau > 23.0$. We use the ISCCP classification (cirrus, cirrostratus, and deep convective clouds) to classify the results provided in the MOD08_D3 (MYD08_D3) products, but with the following modification. We use two classes for high clouds, one for cirriform clouds including cirrus and cirrostratus clouds (Rao et al. 1990; Chou and Neelin 1999; Cartalis et al. 2004), and the other for deep convective clouds.

3. Results

3.1 Average high cloud properties

The three-year mean properties of all high clouds as well as the subgroups of cirriform and deep convective clouds are listed in Table 1. The high cloud properties over ocean and land from Terra (descending orbit, equatorial crossing time of 1030 LST) and Aqua (ascending orbit, equatorial crossing time of 1330 LST) are provided separately. Based on these statistics, we investigate potential differences between the results over land and ocean as well as the diurnal variations of cloud properties.

For all high clouds, the means of high cloud fraction, cloud-top pressure, cloud-top temperature, optical thickness, effective radius, and effective emissivity are 22.7%, 280 hPa, 231 K, 12.8, 26.5 μm , 0.69, respectively. Some general features are noted for all high clouds. First, the total high cloud fraction is higher over land than ocean for both morning (Terra) and afternoon (Aqua) observations. However, the high cloud fraction tends to increase from morning to afternoon. Cloud-top pressure and cloud-top temperature have higher values over land than ocean for both Terra and Aqua. In contrast, high cloud effective radius and effective emissivity have larger values over ocean. Cloud optical thickness and effective particle size display both land-ocean and morning-afternoon differences. Both optical thickness and effective radius have larger values in the morning over ocean while the largest values occur over land in the afternoon.

The mean value of the total high cloud fraction (22.7%) from both MODIS Terra and Aqua platforms is in agreement with that determined from the ISCCP data (Rossow and Schiffer 1999), which has a mean value of high cloud fraction in daytime over the tropics of 23.8%. However, it is important to note that the time coverage of ISCCP and MODIS is not the same. The underestimation of high cloud fraction by the MODIS with respect to the ISCCP is only about 1%. This is mostly due to different thresholds of detectable thin cirrus cloud (Jin et al. 1996; Wylie and Wang 1997; Rossow and Schiffer 1999; Stubenrauch et al. 1999). Zhang et al. (2005) found that the different minimum detectable thresholds of cloud optical thickness could lead to large differences in cloud fraction. Of the total high cloud fraction, the primary contribution is from the cirriform cloud class, which contributes over 80% of the total high cloud fraction. This is

consistent with the ISCCP results indicating that high clouds are mainly cirrus. The value of the deep convective cloud fraction from the MODIS is 3.8, which is close to the value (~2.7) derived from the ISCCP (Rossow and Shiffer 1999).

Cirriiform clouds have higher values of cloud fraction, cloud top pressure, cloud top temperature, and optical thickness over land than over ocean, whereas they have larger values of effective radius and effective emissivity over ocean. One interesting feature is that the differences between the cirriiform cloud fraction over land and ocean in the morning are approximately twice those in the afternoon. The cirriiform cloud fraction over land tends to decrease slightly from morning (24.5) to afternoon (23.3), while the cirriiform cloud fraction over ocean increases from 15.9 to 18.7.

Deep convective clouds over land have higher values of cloud fraction, cloud-top pressure, cloud-top temperature, and optical thickness than those over ocean in both the morning and afternoon. However, deep convective cloud effective radius and effective emissivity values are in contrast. The deep convective cloud fraction over land increases by almost a factor of 1.5 from morning to afternoon. Over ocean, the deep convective cloud fraction has its maximum in the morning and decreases slightly from morning to afternoon. The morning-afternoon and land-ocean contrasts are in agreement with those based on satellite precipitation radar and infrared sensor data (Alcala and Dessler 2002; Hong et al. 2006).

Figures 1-3 show the frequency distributions of cloud-top temperature, effective emissivity, optical thickness, and effective radius for all high clouds as well as the cirriiform and deep convective cloud classes over ocean and land for the tropics (30°S–30°N) from Terra and Aqua. The histograms of the high cloud-top temperatures generally

are flat in the range of 220–240 K (Figures 1a and b). The land-ocean contrast of the distributions in the afternoon is pronounced. The maximum frequency of high cloud-top temperature occurs over land at about 235 K and over ocean at about 222 K. The frequency distribution of high cloud effective emissivity (Figures 1c and d) displays a maximum at about 0.92 in the afternoon. The land-ocean contrast of the frequency distribution of high cloud effective emissivity in the morning is pronounced. The high cloud effective emissivity has a maximum frequency at approximately 0.9, with the exception being in the morning over land, where the maximum frequency is approximately 0.68. The highest frequency of high cloud optical thickness occurs at values between 2 and 3 (Figures 1e and f). This indicates that most high clouds are optically thin. The peak in the frequencies of total high cloud optical thickness occurs at a larger optical thickness over land than over ocean. The peak in high cloud effective radius peaks at about 29 μm over ocean but at slightly smaller values over land (Figures 1g and h). The morning-afternoon contrast is pronounced for high cloud-top temperature, effective emissivity, and effective radius over land.

The frequency distributions over-ocean are much narrower than those over land. The frequency distributions of cirriform cloud-top temperature, optical thickness, and effective radius (Figures 2a, b, and e-h) have similar features as those for total high clouds. Cirriform cloud effective emissivities have their maximum frequencies at larger values over ocean than those over land (Figures 2c and d). The frequency distributions in the afternoon have a pronounced land-ocean contrast. The morning-afternoon contrast is pronounced over ocean for high cloud top temperature and effective emissivity, whereas the contrast is more pronounced over land for effective radius.

The frequencies of deep convective cloud top temperatures (Figures 3a and b) are generally flat in the range of 200–250 K with a slight peak at 202 K in the morning and at about 220 K in the afternoon, whereas those over ocean appear at about 202 K in the morning and about 208 K in the afternoon. Moreover, the frequencies have narrower distributions in the morning. Significant morning-afternoon contrast of the deep convective cloud-top temperature is found over both ocean and land. Deep convective cloud effective emissivities (Figures 3c and d) have a peak in the frequency distribution at 0.88 in the morning and 0.94 in the afternoon. Deep convective cloud optical thicknesses (Figures 3e and f) have a peak in frequency at a value of approximately 23, which is the lowest threshold value used to identify deep convective clouds. Different from total high clouds (Figures 1g and h) and cirriform clouds (Figures 2g and h) showing sharper land-ocean contrasts in their frequency distributions of effective radii in both the morning and the afternoon, deep convective clouds (Figures 3g and h) only show a land-ocean contrasts in the afternoon. All deep convective clouds have their maximum frequencies at 27–28 μm . The deep convective clouds over land in the morning have a distinct feature that is interesting, a secondary peak of their frequency distribution at around 13 μm . Deep convective cloud effective radii also show significant morning-afternoon contrast over land.

Figure 4 shows the monthly variation of the high cloud fraction, effective emissivity, optical thickness, and effective radius for the three-year period from Terra and Aqua over the tropics. In general, the monthly variations over the same underlying surface (ocean or land) from Terra and Aqua have similar changes with months. No obvious trends are observed in the monthly variations for the three years. The high cloud

fraction does show seasonal variations that are consistent with the high cloud survey based on eight years of HIRS data (Wylie and Menzel 1999). The high cloud effective emissivities and optical thicknesses (Figures 4b and c) also have distinct seasonal variations over land. The high cloud effective radii (Figure 4d) display very weak variations. The land-ocean and morning-afternoon contrasts are also evident but are essentially consistent with those in Table 1.

3.2. Geographical high cloud distributions

Figure 5 shows the geographical distribution of the three-year mean fractions for total high cloud, cirriform, and deep convective clouds from Terra and Aqua over the tropics. The distributions of these three cloud groups in the morning (left panels) are similar to those in the afternoon (right panels). Furthermore, high clouds concentrate over the Intertropical Convergence Zone (ITCZ), the South Pacific Convergence Zone (SPCZ), tropical Africa, Indian Ocean, and tropical and South America. These geographical distributions agree well with those reported by many previous studies (e.g., Wylie et al. 1994; Wylie and Menzel 1999; Alcala and Dessler 2002; Jiang et al. 2004; Luo and Rossow 2004; Tian et al. 2004; Wylie et al., 2005; Hong et al. 2005, 2006; Stubenrauch et al., 2006). Additionally, the distribution of cirriform and deep convective clouds suggests that cirriform clouds tend to occur in conjunction with tropical deep convective systems.

From morning (Figure 5, left panels) to afternoon (Figure 5, right panels), total high cloud and cirriform fractions increase strongly over the western Pacific and Indian Oceans where these clouds occur frequently. Cirriform cloud fractions generally decrease

over land. In contrast to the case for cirriform clouds, deep convective cloud fractions generally decrease over ocean and increase over land. These morning-afternoon variations in cloud fraction are consistent with the corresponding features of their three-year means in Table 1. From morning to afternoon over ocean, the increase of cirriform clouds occur in conjunction with the decrease of deep convective clouds. From morning to afternoon over land, the heating of land surface enhances the instability of the atmosphere (Jin and Dickinson 2000), and leads to the development of deep convective clouds. Over the Indonesian maritime region, cirriform clouds occur frequently over maritime continents in the morning. Deep convective clouds over this region display a larger land-ocean contrast in the morning than in the afternoon while they appear to have the opposite relationship over South America. This shows that the different diurnal cycles of deep convective clouds over the western Pacific ocean peaking in the morning from those over land peaking in the afternoon (e.g., Chen and Houze 1997).

Figures 6 and 7 show the geographical distribution of three-year means of high cloud optical thickness, effective radius, effective emissivity, and cloud-top temperature from Terra and Aqua, respectively. The geographical distributions from Terra are similar to those from Aqua. The large values of high cloud optical thicknesses occur over Africa, the Indian Ocean, Southern Asia, the ITCZ, the SPCZ, Australia, and South America. High cloud optical thicknesses show a second ITCZ over the eastern Pacific Ocean (Figures 6a and 7a). The dense concentrations of large ice cloud effective radii appear over ocean (Figures 6b and 7b). The features of the distributions of high cloud effective emissivity are consistent with those for high cloud optical thickness (Figures 6c and 7c). The frequency of large values of ice cloud effective emissivity tends to increase towards

high latitudes. Low high cloud top temperatures are in general associated with higher cloud fractions (Figures 6d and 7d).

The morning-afternoon contrasts of high cloud optical thickness, effective radius, and top temperature are evident and are generally consistent with those of the three-year means over the entire tropics presented in Table 1. High cloud optical thickness (Figures 6a and 7a) and effective radius (Figures 6b and 7b) have pronounced land-ocean contrasts. The land-ocean contrast of high cloud optical thickness increases from morning (Figure 6a) to afternoon (Figure 7a). However, the land-ocean contrast of high cloud effective radius decreases from morning to afternoon. Those distinct land-ocean contrasts are also consistent with the results listed in Table 1.

3.3. Seasonal high cloud distributions

Figure 8 shows the seasonal distributions of the Terra and Aqua MODIS high cloud fraction, optical thickness, and effective radius in the northern hemisphere summer and winter seasons. The months of June, July, and August (JJA) are denoted as summer in the northern hemisphere (austral winter) and the months of December, January, and February (DJF) are denoted as winter in the northern hemisphere (austral summer). The seasonal high cloud optical thicknesses (Figures 8c and d) and effective radii (Figures 8e and f) are averaged over the regions where the high cloud fractions are above 0.5%. The white regions in these figures denote areas in which the high cloud fractions are less than 0.5%. As expected, the ITCZ is indicated by high cloud fractions (Figures 8a and b), and moves south with the sun from summer to winter. This is in agreement with many previous studies (e.g., Wylie et al. 1994; Jin et al. 1996; Wylie and Menzel 1999; Tian et

al. 2004; Wylie et al., 2005; Hong et al. 2005; Stubenrauch et al., 2006). High cloud optical thicknesses (Figures 8c and d) do not show the distinct seasonal variation as high cloud fractions. In winter, the highest values of optical thickness appear over Southeast Asia. High cloud optical thicknesses tend to be large along the Andes Mountains in both summer and winter. Over Africa and the tropical Atlantic, the high values of cloud optical thickness tend to shift south from summer to winter. High cloud effective radii (Figures 8e and f) generally have a southern shift from summer to winter. The land-ocean contrasts of cloud effective radii are very pronounced. Moreover, the largest cloud effective radii occur over the south Pacific and Atlantic in summer. The largest values of cloud effective radii are located over the Arabian Sea, Bay of Bengal, and southwest coast of central America in winter.

To study the seasonal cycle in more detail, the monthly means of cloud fraction, optical thickness, effective radius, cloud-top temperature, and effective emissivity of high cloud and cirriform and deep convective clouds from the Terra and Aqua over tropical land and ocean have been averaged over the three-year period and are shown in Figure 9. The morning-afternoon and land-ocean contrasts of these monthly cloud properties agree well with those of the three-year mean properties found in Table 1.

The cloud fractions of the total and cirriform high clouds (Figures 9a and b) have stronger seasonal variations over land than over ocean. The deep convective cloud fractions (Figure 9c) have stronger seasonal variations in the afternoon than in the morning. The monthly cloud fractions of the total and cirriform high clouds in the afternoon are similar to those in the morning. Over both land and ocean, the seasonal variations of cloud fractions of the total and cirriform high clouds generally display

minima in northern hemisphere summer and maxima in winter or spring. Deep convective clouds form less frequently in February and March over ocean, but more frequently in June and November. Over land, the monthly variation of deep convective clouds is more pronounced in the afternoon than in the morning. There are pronounced secondary maxima for cloud fractions over ocean in spring or fall.

The optical thicknesses of total high and cirriform clouds (Figures 9d and e) have stronger seasonal variations over land than over ocean. In general, monthly variations of optical thicknesses have similar trends in the morning and afternoon over the same underlying surface type although the months associated with minima and maxima of cloud optical thicknesses vary over ocean and land in the morning or afternoon. The annual cycles of the high cloud and cirriform cloud fraction and optical thickness appear to be opposite each other over land. The seasonal variations of cloud effective radii are very weak and vary in the range of about 2 μm (Figures 9g–i). Cloud-top temperatures (Figures 9j–l) vary in the range of about 5 K. Cloud effective emissivity (Figures 9m–o) generally displays stronger seasonal variations over land. Over ocean, they have slightly stronger seasonal variations in the afternoon. Over land, high cloud and cirriform cloud effective emissivity displays a maxima in summer and minima in winter. The effective emissivities of deep convective clouds have pronounced seasonal variations only over land in the morning and over ocean in the afternoon.

3.4. Zonal means of high cloud properties

The zonal means as a function of latitude of cloud fraction, optical thickness, and effective radius for tropical total high cloud as well as cirriform and deep convective

cloud are shown in Figure 10. The zonal means are shown separately over land and ocean from Terra and Aqua for the boreal summer and winter to investigate the land-ocean contrast and seasonal variations.

Figure 10a shows the distribution of high cloud properties with latitude. In summer, the peak in high cloud fraction occurs between 8–10°N; the lowest values are found near 18°S. Additionally, the latitudes corresponding to the highest and lowest cloud fractions over land in the same seasons differ from those over ocean by a few degrees. The seasonal shifting of high cloud fractions is consistent with the results shown in Figure 8. The high cloud fractions in winter have a unique feature of distinct double peaks between 15°S and 15°N over land and between 10°S and 10°N over ocean. The variation of high cloud fraction with latitude is larger over ocean than over land in summer, but the situation is reversed for winter. The seasonal shifting of high cloud optical thickness (Figure 10b) is not as regular as that of high cloud fraction. High cloud optical thicknesses show stronger variation with latitude over land, as do high cloud effective radii (Figure 10c). Large values of high cloud effective radii over land occur near the equator and extend to higher latitudes in the southern hemisphere. High cloud effective radii over ocean in winter weakly depend on the latitudes, whereas those over ocean during the summer have their largest values near the equator.

Cirriform cloud fractions (Figure 10d) have similar distributions as the total high cloud. The variation of cirriform cloud optical thickness (Figure 10e) over land is much stronger than over ocean in both summer and winter. The distributions of cirriform cloud effective radii (Figure 10f) are similar to those for all high clouds. The distribution of deep convective clouds (Figure 10g) is similar to those for total high clouds and cirriform

clouds except over land in summer, which have a peak at 30°N. The deep convective cloud fractions over ocean in summer also have a slightly secondary peak near 6°S. Over land, the deep convective cloud fractions vary more with latitude in winter than in summer. However, the deep convective cloud fractions over ocean vary less with latitude in winter than in summer. The influence of midlatitude storm belts on the deep convective cloud fraction is evident. At high latitudes (30°S and 30°N), the deep convective cloud fractions tend to be larger. The deep convective cloud optical thicknesses (Figure 10h) are higher over land in both summer and winter. Over ocean, the deep convective cloud optical thicknesses tend to decrease from 30°S to 30°N in summer and decrease from 30°S to 30°N in winter. The deep convective cloud effective radii (Figure 10i) show more latitudinal variation over land than over ocean in both summer and winter. However, their summer-winter contrasts are quite pronounced over both land and ocean.

4. Conclusions

The MODIS measurements from the Terra and Aqua platforms provide an unprecedented opportunity to study the climatology of high cloud properties. Three years (September 2002 through August 2005) of the MODIS Collection 4 Level-3 cloud products are analyzed with a focus on high (ice) clouds. The cloud properties include cloud fraction, cloud optical thickness, effective radius, cloud-top temperature, cloud-top pressure, and effective emissivity. We investigate the characteristics of all high ice clouds over the tropics (30°S–30°N) as well as sub-classes designated as cirriform and deep convective clouds based on the ISCCP classification approach. Because the retrieved

cloud properties are sensitive to the retrieval algorithms and satellite sensors used (Wielicki and Parker 1992), the present results are complementary to the cloud climatologies derived from the previous studies reported in the literature.

The three-year mean properties of high clouds over ocean and land in the morning (Terra) and afternoon (Aqua) are discussed. Over 80% of all high clouds are noted to be cirriform clouds. The land-ocean and morning-afternoon contrasts are pronounced for cloud properties of all high clouds as well as cirriform and deep convective clouds. High clouds appear more frequently over land and in the afternoon. However, they tend to have higher cloud-top heights, larger effective radii, and stronger effective emissivities over ocean. From morning to afternoon, the effective radii and optical thicknesses increase over land and decrease over ocean. The land-ocean contrast of cirriform cloud fraction is much stronger in the morning than in the afternoon. Deep convective clouds have a stronger land-ocean contrast in the afternoon. Cirriform and deep convective clouds have larger values of cloud fraction, cloud-top pressure, cloud-top temperature, and optical thickness but smaller values of effective radius and effective emissivity over land than over ocean. No evident trends are observed in the monthly variations of high cloud properties from the three-year data. However, high cloud fraction, effective emissivity, and optical thickness show stronger seasonal variations, particularly over land. They also show pronounced morning-afternoon and land-ocean contrasts.

The geographical distribution of cloud fraction of all high clouds as well as cirriform and deep convective clouds have similar patterns. High clouds are concentrated over the ITCZ, SPCZ, tropical Africa, Indian Ocean, and tropical and South America. Over ocean, the increase of cirriform clouds occurs in conjunction with the decrease of

deep convective clouds, whereas over land, the decrease of cirriform clouds occurs in conjunction with the increase of deep convective clouds. The geographical distribution of high cloud properties from Terra are similar to those from Aqua. The highest values of high cloud optical thickness occur over land while the largest effective radii occur over ocean. The effective emissivities of high clouds tend to increase toward higher latitudes. The high cloud fraction has a distinct seasonal shift to the south from the northern hemisphere from boreal summer to winter. The geographical distributions of the optical thicknesses and effective radii of these clouds also show seasonal variations. The land-ocean and summer-winter contrasts are also found in the zonal means of the various cloud properties.

Acknowledgements

This effort is supported by a NASA research grant (NNG04GL24G) from NASA Radiation Sciences Program managed by Dr. Hal Maring (previously by Dr. Donald Anderson) and the MODIS program managed by Dr. Paula Bontempi. This study is also partially supported by the National Science Foundation Physical Meteorology Program (ATM-0239605) managed by Dr. Andrew Detwiler, and a NASA research grant (NNG05GL78G). We thank the three anonymous reviewers for constructive comments and helpful suggestions.

References

- Alcala, C. M., and A. E. Dessler, 2002: Observations of deep convection in the tropics using the Tropical Rainfall Measuring Mission (TRMM) precipitation radar. *J. Geophys. Res.*, **107**, 4792, doi:10.1029/2002JD002457.
- Barnes, W. L., T. S. Pagano, and V. V. Salomonson, 1998: Prelaunch characteristics of the Moderate Resolution Imaging Spectroradiometer (MODIS) on EOS-AM1. *IEEE Trans. Geosci. Remote Sens.*, **36**, 1088–1100.
- Baum, B. A., A. J. Heymsfield, P. Yang, and S. T. Bedka, 2005a: Bulk scattering models for the remote sensing of ice clouds. Part I: Microphysical data and models. *J. Appl. Meteor.*, **44**, 1885–1895.
- Baum, B. A., P. Yang, A. J. Heymsfield, S. Platnick, M. D. King, Y.-X. Hu, and S. T. Bedka, 2005b: Bulk scattering models for the remote sensing of ice clouds. Part II: Narrowband models. *J. Appl. Meteor.*, **44**, 1896–1911.
- Baum, B. A., P. F. Soulen, K. I. Strabala, M. D. King, S. A. Ackerman, and W. P. Menzel, 2000: Remote sensing of cloud properties using MODIS airborne simulator imagery during SUCCESS. II. Cloud thermodynamic phase. *J. Geophys. Res.*, **105**, 11,781–11,792.
- Cartalis, C., N. Chrysoulakis, H. Feidas, and N. Pitsitakis, 2004: Categorization of cold period weather types in Greece on the basis of the photointerpretation of NOAA/AVHRR imagery. *Int. J. Remote Sensing*, **25**, 2951–2977.
- Chen, S. S., and R. A. Houze Jr., 1997: Diurnal variation and lifecycle of deep convective systems over the tropical Pacific warm pool. *Quart. J. Roy. Meteor. Soc.*, **123**, 357–388.

- Chou, C., and J. D. Neelin, 1999: Cirrus detrainment-temperature feedback. *Geophys. Res. Lett.*, **26**, 1295–1298.
- Chung, S., S. Ackerman, P. F. van Delst, and W. P. Menzel, 2000: Model calculations and interferometer measurements of ice-cloud characteristics. *J. Appl. Meteorol.*, **39**, 634–644.
- Dessler, A. E., and P. Yang, 2003: The distribution of tropical thin cirrus clouds inferred from Terra MODIS data. *J. Climate*, **16**, 1241–1247.
- Foot, J. S., 1988: Some observations of the optical properties of clouds. Part II: Cirrus, *Quart. J. Roy. Meteor. Soc.*, **114**, 145–164.
- Hong, G., G. Heygster, J. Miao, and K. Kunzi, 2005: Detection of tropical deep convective clouds from AMSU-B water vapor channels measurements. *J. Geophys. Res.*, **110**, D05205, doi:10.1029/2004JD004949.
- Hong, G., G. Heygster, and C. A. M. Rodriguez, 2006: Effect of cirrus clouds on the diurnal cycle of tropical deep convective clouds. *J. Geophys. Res.*, **111**, doi:10.1029/2005JD006208.
- Jensen, E. J., S. Kinne, and O. B. Toon, 1994a: Tropical cirrus cloud radiative forcing: Sensitivity studies. *Geophys. Res. Lett.*, **21**, 2023–2026.
- Jin, M., and R. E. Dickinson, 2000: A generalized algorithm for retrieving cloudy sky skin temperature from satellite thermal infrared radiances. *J. Geophys. Res.*, **105**, 27,037–27,048.
- Jin, Y., W. B. Rossow, and D. P. Wylie, 1996: Comparison of the climatologies of high-level clouds from HIRS and ISCCP. *J. Climate*, **9**, 2850–2879.
- Jiang, J. H., B. Wang, K. Goya, K. Hocke, S. D. Eckermann, J. Ma, D. L. Wu, and W. G. Read, 2004: Geographical distribution and interseasonal variability of tropical

- deep convection: UARS MLS observations and analyses. *J. Geophys. Res.*, **109**, D03111, doi:10.1029/2003JD003756.
- King, M. D., W. P. Menzel, Y. J. Kaufman, D. Tanré, B. C. Gao, S. Platnick, S. A. Ackerman, L. A. Remer, R. Pincus, and P. A. Hubanks, 2003: Cloud and aerosol properties, precipitable water, and profiles of temperature and water vapor from MODIS. *IEEE Trans. Geosci. Remote Sensing*, **41**, 442–458.
- King, M. D., S. Platnick, P. Yang, G. T. Arnold, M. A. Gray, J. C. Riédi, S. A. Ackerman, and K. N. Liou, 2004: Remote sensing of liquid water and ice cloud optical thickness, and effective radius in the arctic: Application of air-borne multispectral MAS data. *J. Atmos. and Ocean. Technol.*, **21**, 857-875.
- Li, J. L., et al., 2005, Comparisons of EOS MLS cloud ice measurements with ECMWF analyses and GCM simulations: Initial results. *Geophys. Res. Lett.*, **32**, L18710, doi:10.1029/2005GL023788.
- Lin, W. Y., and M. H. Zhang, 2004: Evaluation of clouds and their radiative effects simulated by the NCAR Community Atmospheric Model against satellite observations. *J. Climate*, **17**, 3302–3318.
- Liou, K. N., 1986: Influence of cirrus clouds on weather and climate processes: A global perspective. *Mon. Weather Rev.*, **114**, 1167–1199.
- Liu, G., J. A. Curry, and R. Sheu, 1995: Classification of clouds over the western equatorial Pacific Ocean using combined infrared and microwave satellite data. *J. Geophys. Res.*, **100**, 13,811–13,826.

- Liu, G., and J. A. Curry, 1999: Tropical ice water amount and its relations to other atmospheric hydrological parameters as inferred from satellite data. *J. Appl. Meteorol.*, **38**, 1182–1194.
- Lubin, D., B. Chen, D. H. Bromwich, R. C. J. Somerville, W.-H. Lee, and K. M. Hines, 1998: The impact of Antarctic cloud radiative properties on a GCM climate simulation. *J. Climate*, **11**, 447–462.
- Luo, Z., and W. B. Rossow, 2004: Characterizing tropical cirrus life cycle, evolution, and interaction with upper-tropospheric water vapor using Lagrangian trajectory analysis of satellite observations. *J. Climate*, **17**, 4541–4563.
- Macke, A., J. Mueller, and E. Raschke, 1996: Single scattering properties of atmospheric ice crystals. *J. Atmos. Sci.*, **53**, 2813–2825.
- McFarlane, N. A., G. J. Boer, J.-P. Blanchet, and M. Lazare, 1992: The Canadian Climate Centre second-generation general circulation model and its equilibrium climate. *J. Climate*, **5**, 1013–1044.
- McFarquhar, G. M., P. Yang, A. Macke, and A. J. Baran, 2002: A new parameterization of single scattering solar radiative properties for tropical anvils using observed ice crystal size and shape distributions. *J. Atmos. Sci.*, **50**, 2458–2478.
- Ou, S. C., and K. N. Liou, 1995: Ice microphysics and climatic temperature feedback. *Atmos. Res.*, **35**, 127–138.
- Platnick, S., M. D. King, S. A. Ackerman, W. P. Menzel, B. A. Baum, J. C. Riédi, and R. A. Frey, 2003: The MODIS cloud products: Algorithms and examples from Terra. *IEEE Trans. Geosci. Remote Sensing*, **41**, 459–473.
- Pilewskie, P., and F. P. J. Valero, 1996: How much solar radiation do clouds absorb? *Science*, **271**, 1131–1133.

- Rao, P. K., S. J. Holms, R. K. Anderson, J. S. Winston, and P. E. Lehr, Eds., 1990: *Weather satellites: Systems, data, and environmental applications*. Amer. Meteor. Soc., Boston, 503 pp.
- Ringer, M. A. and R. P. Allan, 2004: Evaluating climate model simulations of tropical cloud. *Tellus*, **56A**, 308–327.
- Rossow, W. B., and R. A. Schiffer, 1991: ISCCP cloud data products. *Bull. Amer. Meteor. Soc.*, **72**, 2–20.
- Rossow, W. B., and R. A. Schiffer, 1999: Advances in understanding clouds from ISCCP. *Bull. Amer. Meteor. Soc.*, **80**, 2261–2287.
- Schiffer, R. A., and W. B. Rossow, 1983: The International Satellite Cloud Climatology Project (ISCCP) – The first project of the World Climate Research Programme. *Bull. Amer. Meteor. Soc.*, **64**, 779–784.
- Salomonson, V.V., W. L. Barnes, P.W. Maymon, H. E. Montgomery, H. Ostrow, 1989: MODIS: advanced facility instrument for studies of the Earth as a system, *IEEE Trans. Geosci. Remote Sensing*, **27**, 145 - 153
- Stephens, G. L., S. C. Tsay, P. W. Stackhouse, and P. J. Flatau, 1990: The relevance of the microphysical and radiative properties of cirrus clouds to climate and climate feedback. *J. Atmos. Sci.*, **47**, 1742–1753.
- Stubenrauch, C. J., W. B. Rossow, F. Chérut, A. Chédin, and N. A. Scott, 1999: Clouds as seen by satellite sounders (3I) and imagers (ISCCP). Part I: Evaluation of cloud parameters. *J. Climate*, **12**, 2189–2213.

- Stubenrauch, C. J., A. Chédin, G. Rädcl, N. A. Scott, and S. Serrar, 2006: Cloud properties and their seasonal and diurnal variability from TOVS. *Submitted to J. Climate*.
- Tian, B., B. J. Soden, and X. Wu, 2004: Diurnal cycle of convection, clouds, and water vapor in the tropical upper troposphere: Satellites versus a general circulation model. *J. Geophys. Res.*, **109**, D10101, doi:10.1029/2003JD004117.
- Tselioudis, G., and C. Jakob, 2002: Evaluation of midlatitude cloud properties in a weather and a climate model: Dependence on dynamic regime and spatial resolution. *J. Geophys. Res.*, **107**, 4781, doi:10.1029/2002JD002259.
- Wang, P.-H.; P. Minnis, M. P. McCormick, G. S. Kent, and K. M. Skeens, 1996: A 6-year climatology of cloud occurrence frequency from Stratospheric Aerosol and Gas Experiment II observations (1985-1990). *J. Geophys. Res.*, **101**, 29,407–29,430.
- Wang, P.-H., P. Minnis, M. P. McCormick, G. S. Kent, G. K. Yue, D. F. Young, and K. M. Skeens, 1998: A Study of the vertical structure of Tropical (20°S–20°N) optically thin clouds from SAGE II observations. *Atmos. Res.*, **47-48**, 599–614.
- Wendisch, M., P. Pilewskie, J. Pommier, S. Howard, P. Yang, A. J. Heymsfield, C. G. Schmitt, D. Baumgardner, and B. Mayer, 2005: Impact of cirrus crystal shape on solar spectral irradiance: A case study for subtropical cirrus. *J. Geophys. Res.*, **110**, D03202, doi:10.1029/2004JD005294.
- Wielicki, B. A., B. R. Barkstrom, E. F. Harrison, R. B. Lee, G. L. Smith, and J. E. Cooper, 1996: Clouds and the earth's radiant energy system (CERES): An earth observing system experiment. *Bull. Amer. Meteor. Soc.*, **77**, 853–868.

- Wielicki, B. A., and L. Parker, 1992: On the determination of cloud cover from satellite sensors: The effect of sensor spatial resolution. *J. Geophys. Res.*, **97**, 12,799–12,823.
- Wylie, D. P., D. L. Jackson, W. P. Menzel, and J. J. Bates, 2005: Trends in global cloud cover in two decades of HIRS observations. *J. Climate*, **18**, 3021–3031.
- Wylie, D. P., and W. P. Menzel, 1999: Eight years of high cloud statistics using HIRS. *J. Climate*, **12**, 170–184.
- Wylie, D. P., P. W. Menzel, H. M. Woolf, and K. I. Strabala, 1994: Four years of global cirrus cloud statistics using HIRS. *J. Climate*, **7**, 1972–1986.
- Wylie, D. P., and P.-H. Wang, 1997: Comparison of cloud frequency data from the high-resolution infrared radiometer sounder and the Stratospheric Aerosol and Gas Experiment II. *J. Geophys. Res.*, **102**, 29,893–29,900.
- Wyser, K., 1998: The effective radius in ice clouds. *J. Climate*, **11**, 1793–1802.
- Yang, P., and K. N. Liou, 1996a: Finite-difference time domain method for light scattering by small ice crystals in three-dimensional space. *J. Opt. Soc. Am. A.*, **13**, 2072–2085.
- Yang, P., and K. N. Liou, 1996b: Geometric-optics-integral-equation method for light scattering by nonspherical ice crystals. *Appl. Opt.*, **35**, 6568–6584.
- Zhang, M. H., et al., 2005: Comparing clouds and their seasonal variations in 10 atmospheric general circulation models with satellite measurements. *J. Geophys. Res.*, **110**, D15S02, doi:10.1029/2004JD005021.

TABLE 1. The three-year mean properties of high cloud and cirriform and deep convective clouds from September 2002 to August 2005 over the tropics (30°S–30°N). All properties are based on daytime results from the MODIS aboard Terra and Aqua at the local equatorial crossing times of 10:30 and 13:30, respectively.

Cloud Properties	Terra			Aqua			Terra and Aqua		
	Land	Ocean	Total	Land	Ocean	Total	Land	Ocean	Total
High Cloud									
Fraction (%)	28.8	19.5	21.7	29.3	21.7	23.6	29.1	20.6	22.7
Top pressure (hPa)	298.2	279.9	285.7	286.1	268.6	274.0	292.2	274.3	279.9
Top temperature (K)	234.4	229.9	231.3	232.3	228.7	229.8	233.4	229.3	230.6
Optical thickness	12.7	13.3	13.1	14.7	11.4	12.4	13.7	12.4	12.8
Effective radius (μm)	23.0	28.0	26.4	24.0	27.6	26.5	23.5	27.8	26.5
Effective emissivity	0.66	0.71	0.70	0.65	0.69	0.68	0.66	0.70	0.69
Cirriform Cloud									
Fraction (%)	24.5	15.9	18.0	23.3	18.7	19.9	23.9	17.3	19.0
Top pressure (hPa)	306.0	296.1	299.3	291.8	277.2	281.4	298.9	286.7	290.4
Top temperature (K)	235.5	232.7	233.6	233.3	230.1	231.0	234.4	231.4	232.3
Optical thickness	7.9	7.5	7.6	8.2	7.5	7.7	8.1	7.5	7.7
Effective radius (μm)	22.8	27.9	26.3	23.8	27.6	26.5	23.3	27.8	26.4
Effective emissivity	0.63	0.68	0.66	0.60	0.65	0.64	0.62	0.67	0.65
Deep Convective Cloud									
Fraction (%)	4.3	3.6	3.8	6.0	3.0	3.7	5.2	3.3	3.8
Top pressure (hPa)	254.2	208.8	221.3	264.3	215.1	234.9	259.3	212.0	228.1
Top temperature (K)	227.8	217.5	220.3	228.4	219.9	223.3	228.1	218.7	221.8
Optical thickness	39.9	38.7	39.1	39.9	35.9	37.5	39.9	37.3	38.3
Effective radius (μm)	24.2	28.0	27.0	24.9	27.5	26.4	24.6	27.8	26.7
Effective emissivity	0.84	0.89	0.87	0.86	0.92	0.90	0.85	0.91	0.89

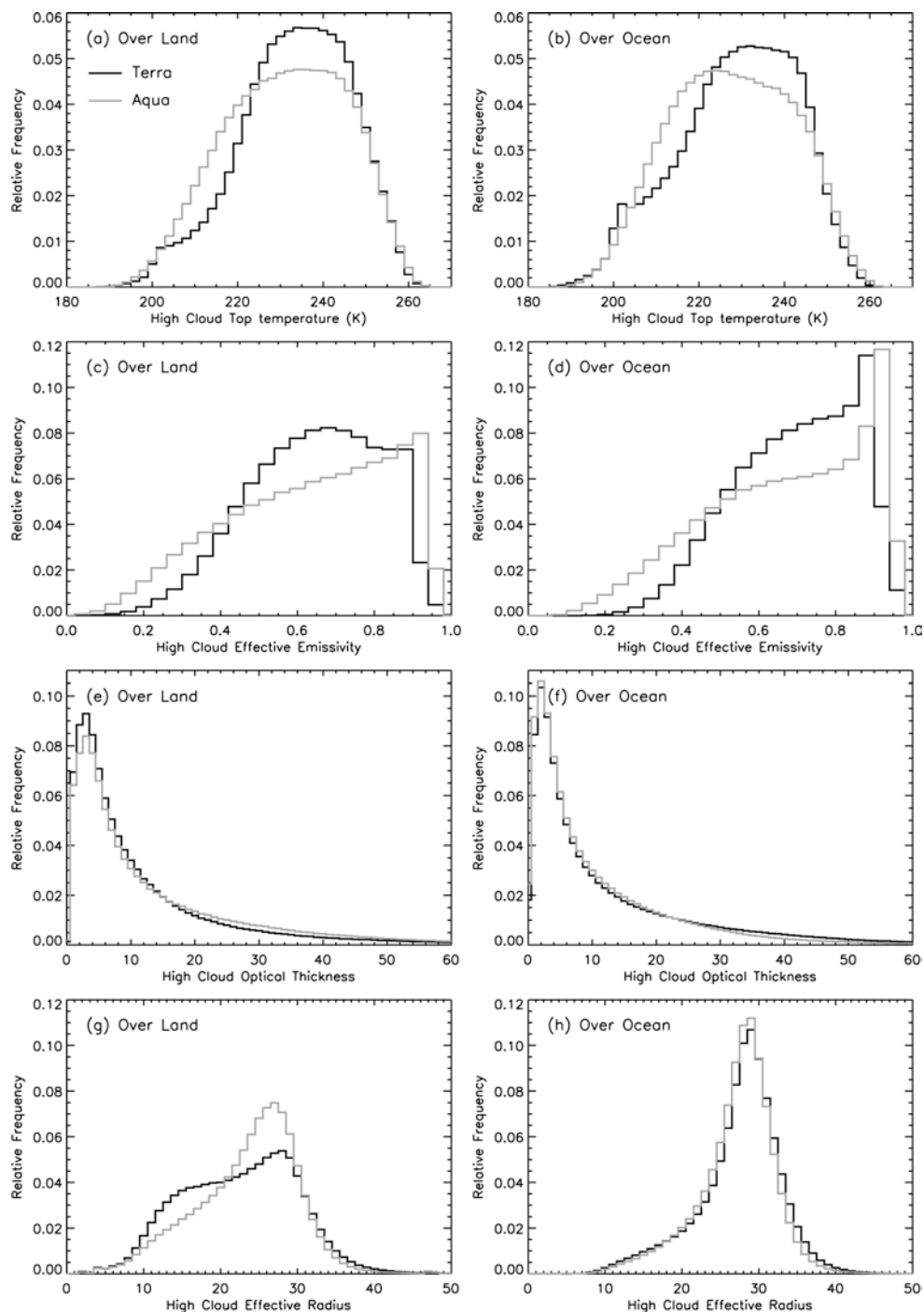


Figure 1. Frequency distributions of cloud-top temperature, effective emissivity, optical thickness, and effective radius for high clouds over ocean and land in the tropics (30°S–30°N) from Terra (descending orbit with an equatorial crossing at 1030 local solar time) and Aqua (ascending orbit with an equatorial crossing at 1330 local solar time).

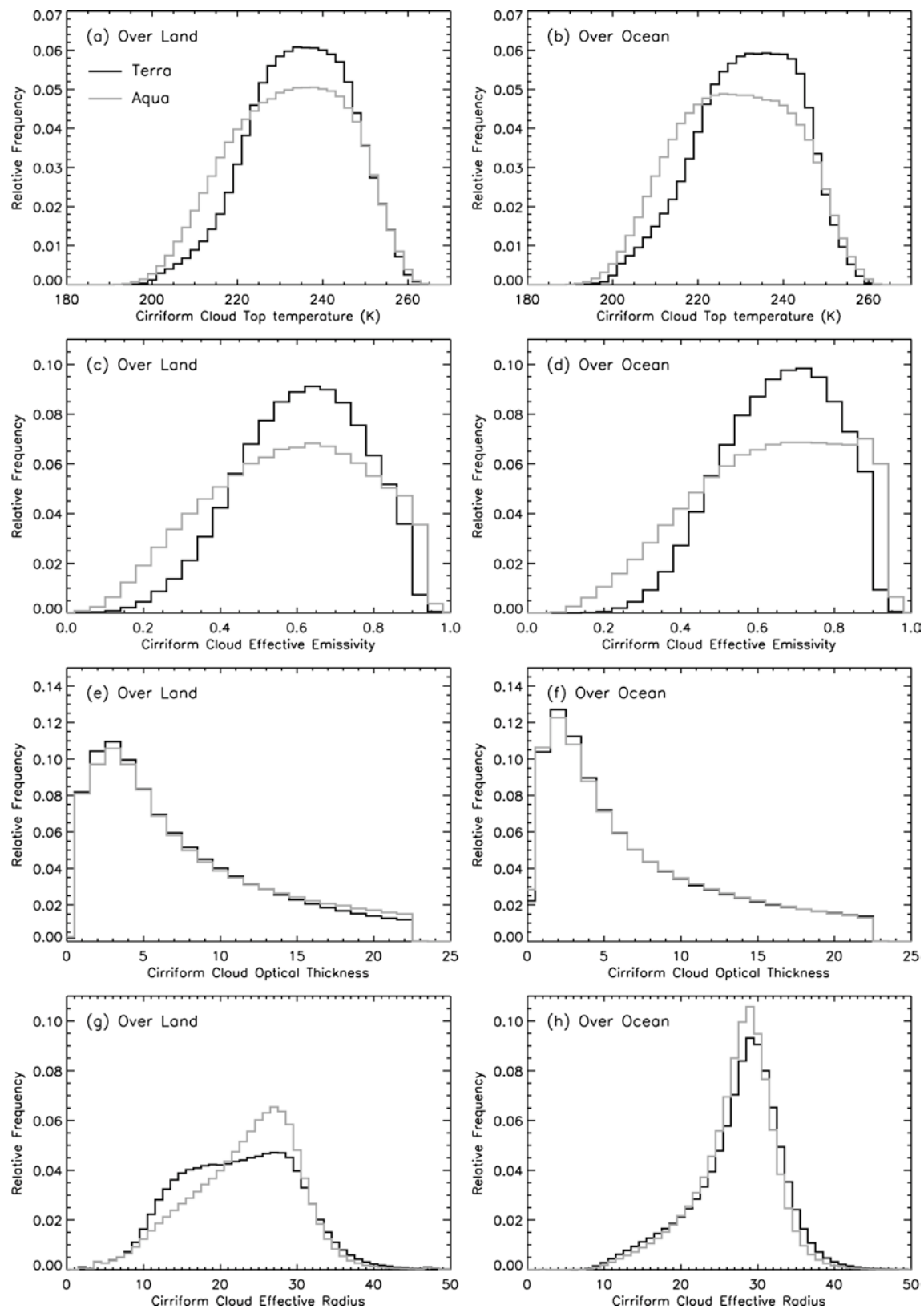


Figure 2. Same as Figure 1, but for cirriform clouds.

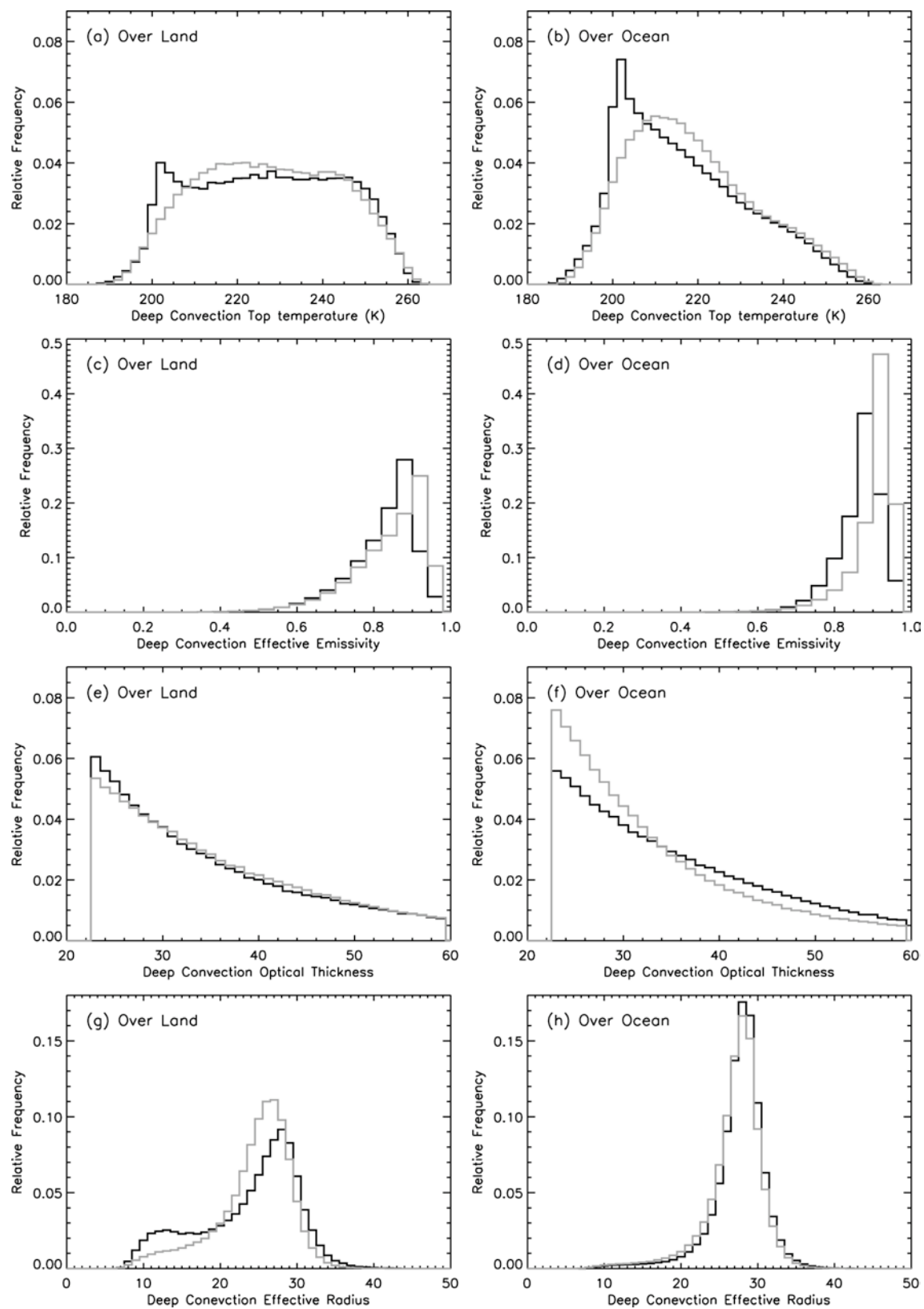


Figure 3. Same as Figure 1, but for deep convective clouds.

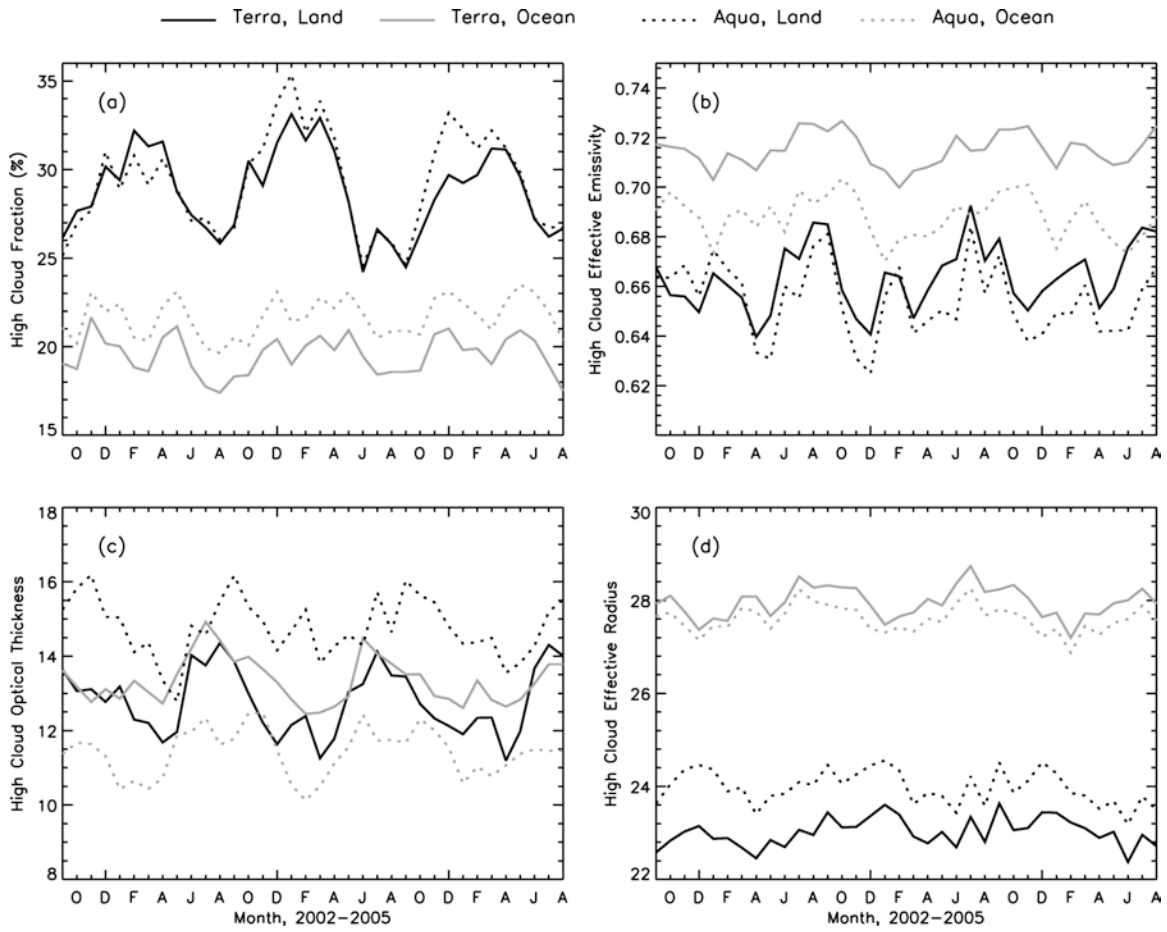


Figure 4. Monthly variations of (a) high cloud fraction, (b) effective emissivity, (c) optical thickness, and (d) effective radius averaged over the tropics (30°S – 30°N) from Terra and Aqua.

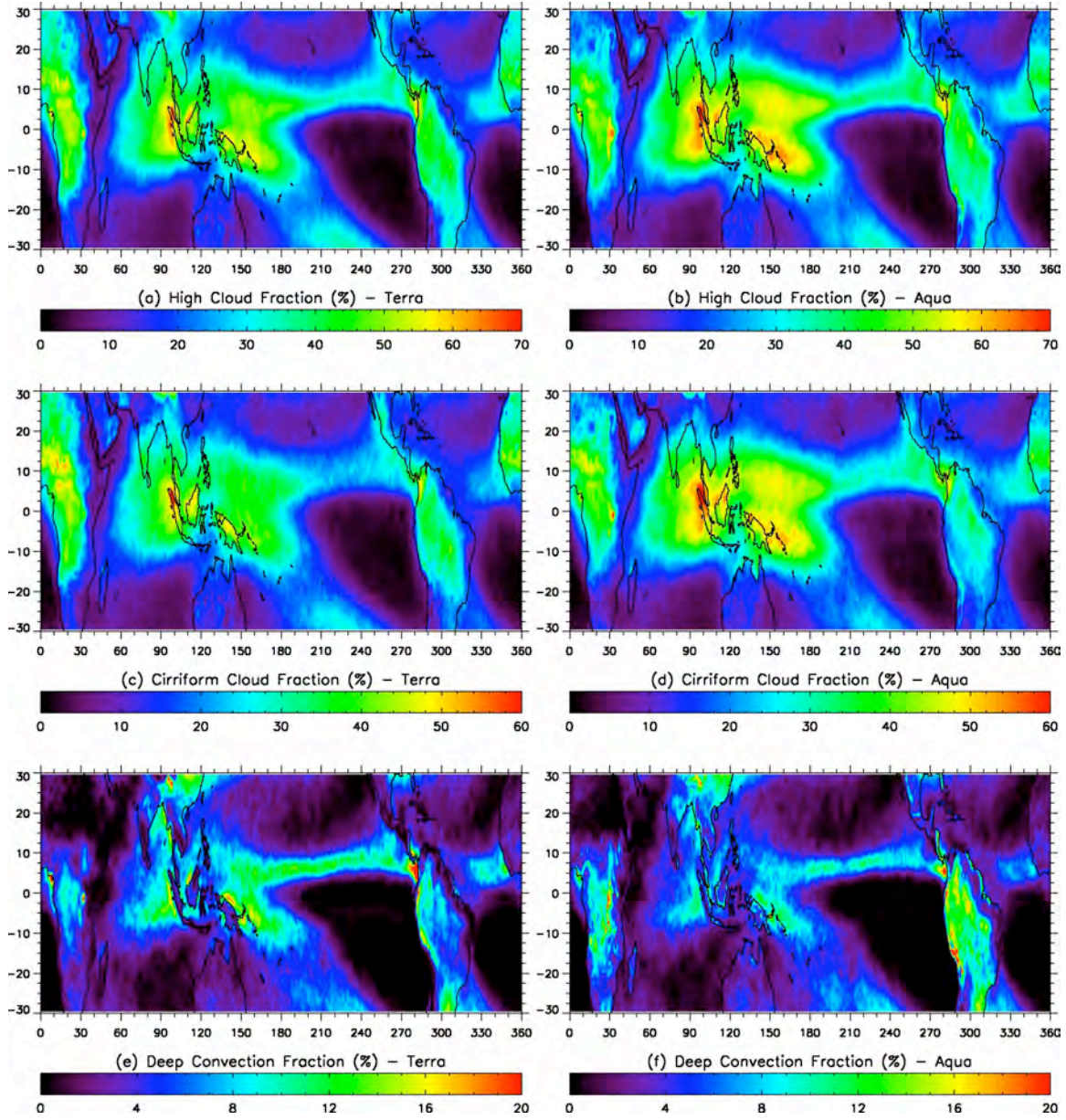


Figure 5. Geographical distributions of the three-year mean fractions of high cloud and cirriform cloud and deep convective cloud from Terra (left panels) and Aqua (right panels) over the tropics (30°S–30°N).

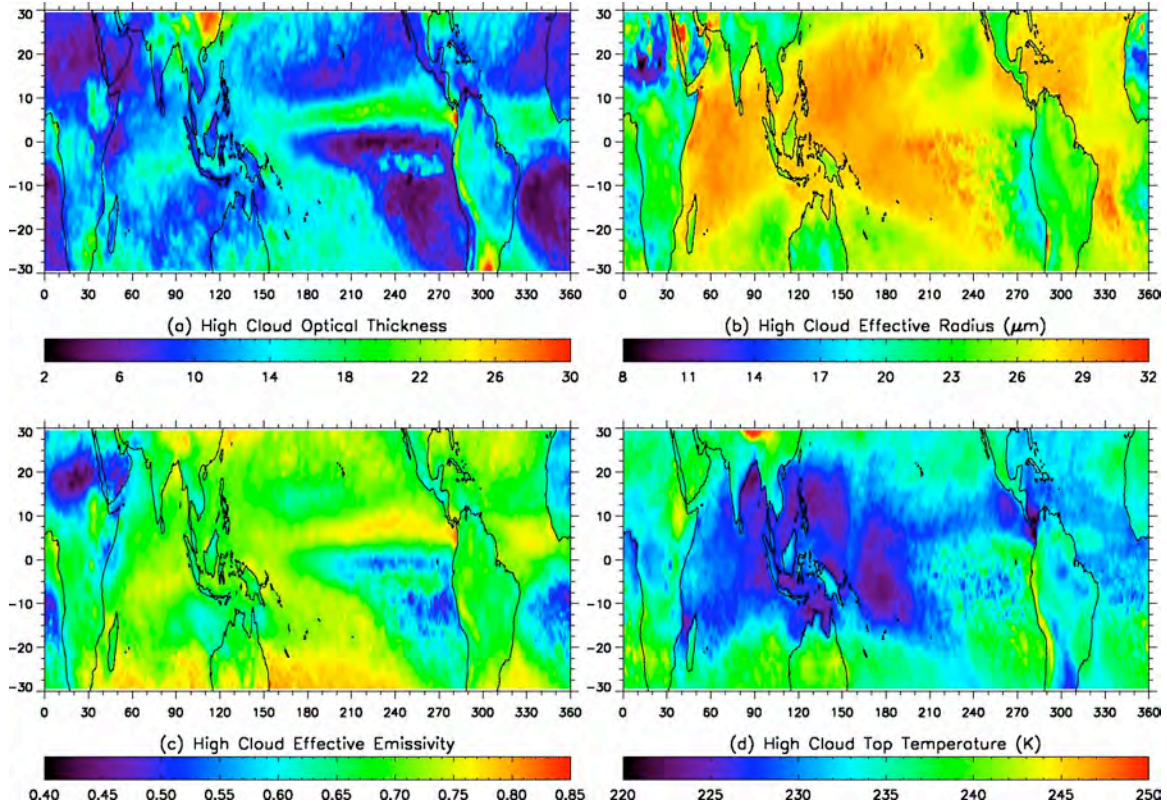


Figure 6. The geographical distributions of three-year means of (a) high cloud optical thickness, (b) effective radius, (c) effective emissivity, and (d) top temperature from Terra over the tropics (30°S–30°N).

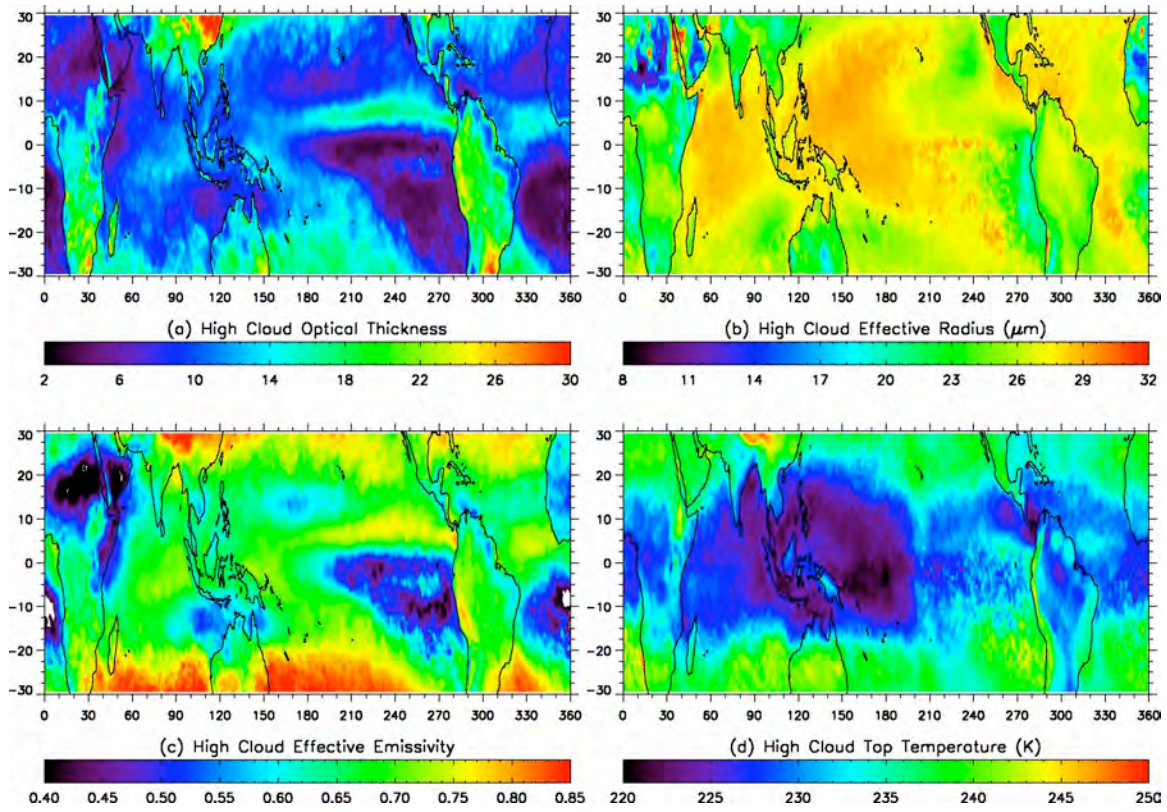


Figure 7. Same as Figure 6, but for Aqua.

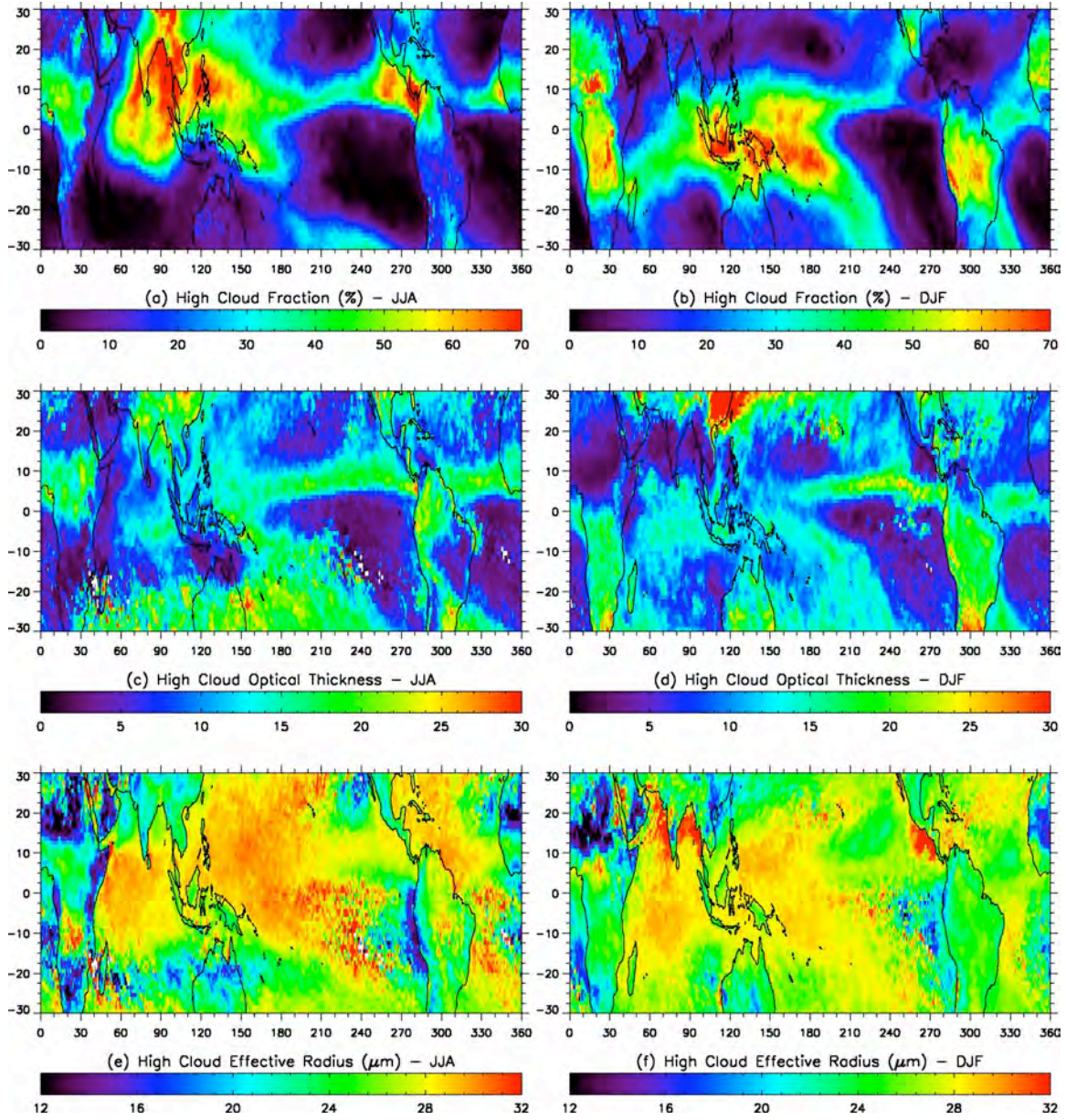


Figure 8. The seasonal distributions of high cloud fraction, optical thickness, and effective radius in the northern hemisphere summer (left panels) and winter (right panels) seasons derived from the three-year Terra and Aqua data over the tropics (30°S–30°N).

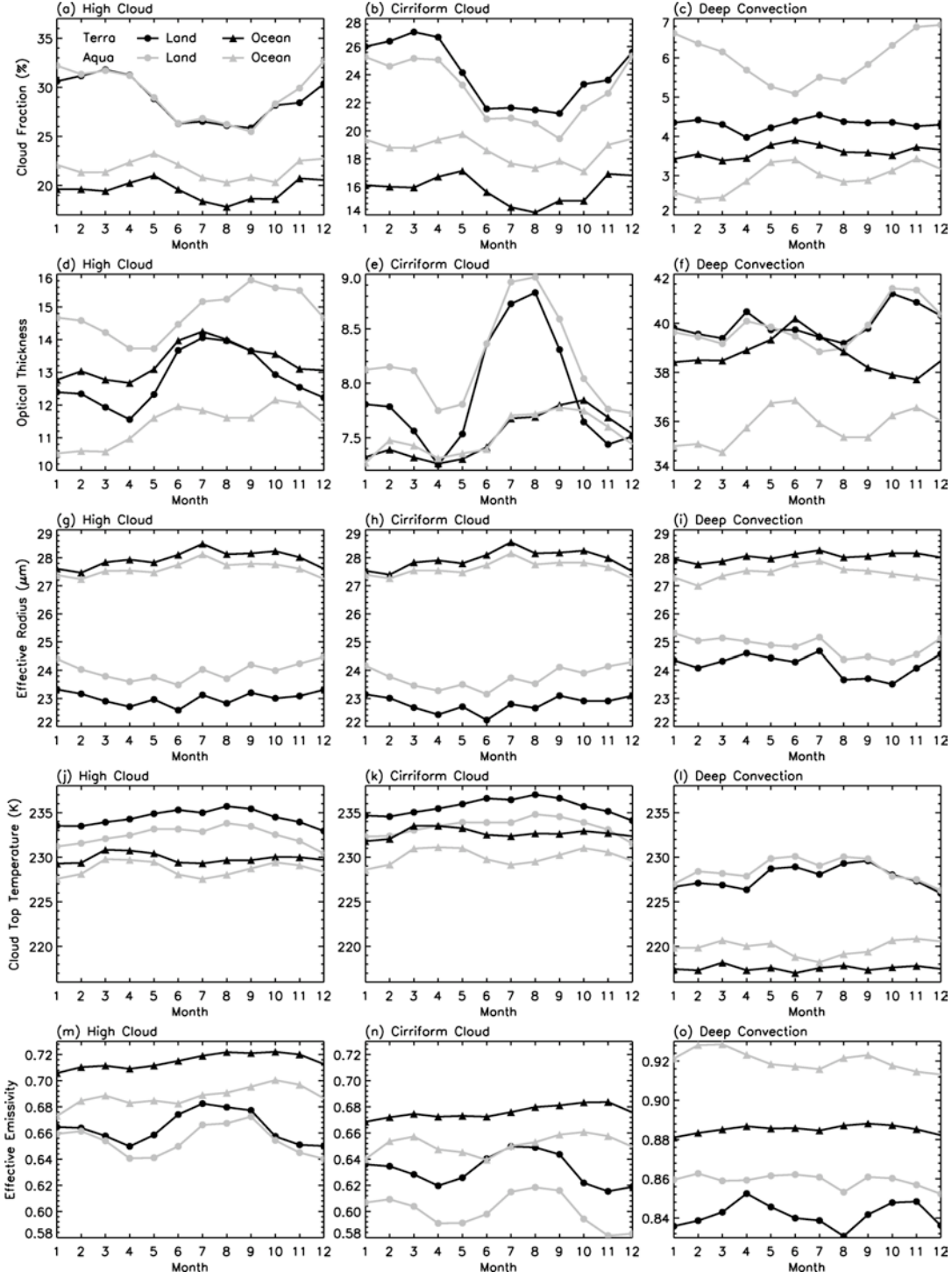


Figure 9. Seasonal variation of cloud fraction, optical thickness, effective radius, cloud-top temperature, and effective emissivity of high cloud and cirriform and deep convective clouds from the Terra and Aqua over the tropical land and ocean (30°S–30°N).

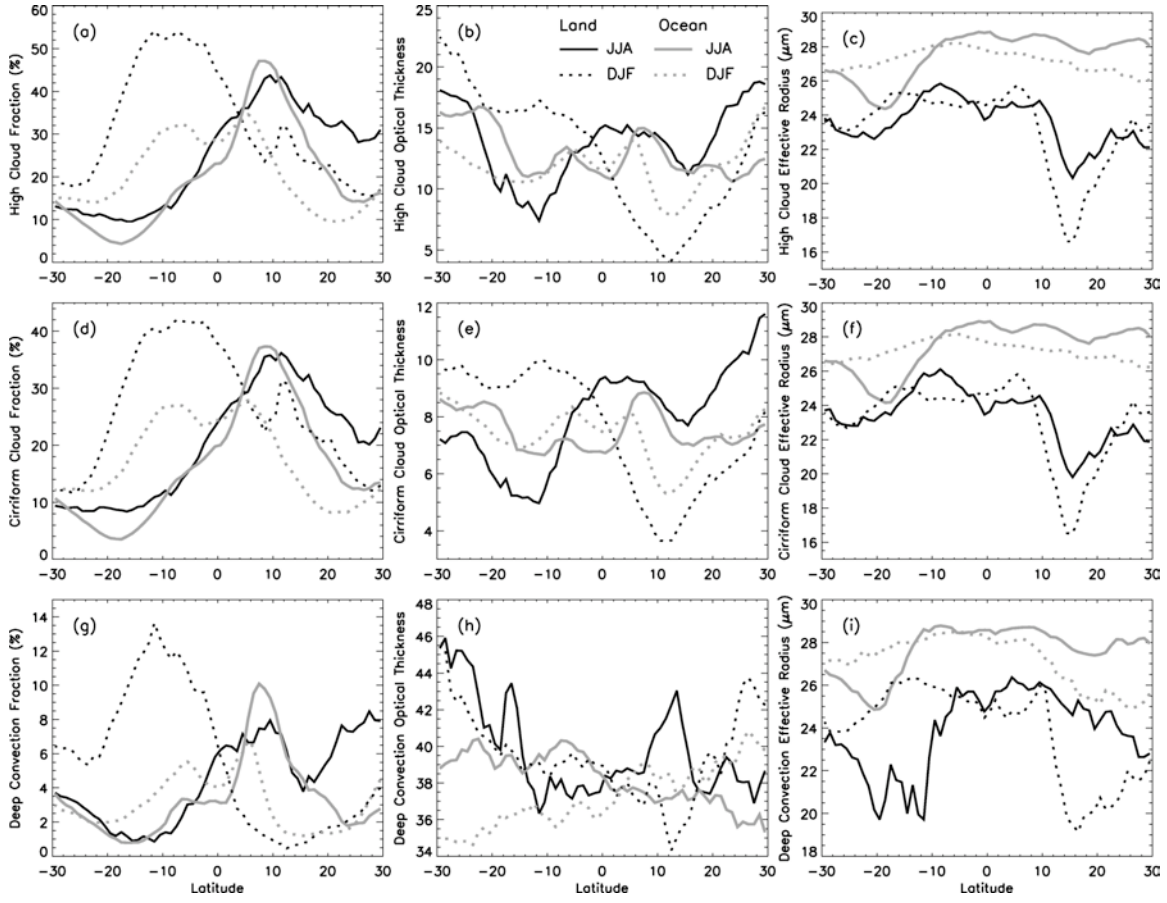


Figure 10. The zonal means cloud properties of tropical high cloud and cirriform and deep convective clouds over land and ocean along latitudes in summer (JJA) and winter (DJF).